Title:

A methodological framework for assessing neural control of shoulder muscles during multi-directional isometric tasks using high-density surface electromyography.

Authors:

J Greig Inglis[1], Silvia Rio[1], Hélio V. Cabral[1,2,3], Caterina Cosentino[1], Roberto Pagani[4], Clark R Dickerson[5], Francesco Negro[1]

Affiliations:

[1]Department of Clinical and Experimental Sciences, Università degli Studi di Brescia, Brescia, Italy

[2]School of Physical Education and Sports, Universidade Federal do Rio de Janeiro, Rio de Janeiro, Brazil

[3]Biomedical Engineering Program (COPPE), Universidade Federal do Rio de Janeiro, Rio de Janeiro, Brazil

[4]Department of Mechanical and Industrial Engineering, Università degli Studi di Brescia, Brescia, Italy

[5]Department of Kinesiology and Health Sciences, University of Waterloo, Waterloo, Canada

Conflict of Interest:

The authors report no conflict of interest.

Acknowledgements:

The authors would like to thank Dr. Tea Lulic-Kuryllo for her input in the protocol and array placement which were integral to the design of the data collection.

Funding:

This study was funded by the European Research Council Consolidator Grant 'INcEPTION', contract no. 101045605. J Greig Inglis was supported by the Marie Skłodowska-Curie Actions Grant 'MUDecomp', agreement no. 101151712.

Corresponding author:

Prof. Francesco Negro

Department of Clinical and Experimental Sciences,

Università degli Studi di Brescia

Viale Europa 11, Brescia, 25121, Italy

Email: francesco.negro@unibs.it

ABSTRACT

The complex movements of the shoulder rely on the coordinated activation of large muscles including the deltoid, pectoralis major, trapezius and latissimus dorsi. However, detailed knowledge of their neuromuscular control remains limited. This study aimed to develop a methodological framework to investigate the neural control of shoulder muscles by combining a 6-degree-of-freedom load cell attached to an industrial robotic arm with high-density surface electromyograms (HDsEMG). Six healthy participants performed isometric contractions (abduction, adduction, flexion and extension) at 30% of maximal voluntary contraction with the shoulder positioned at 30° and 65° of lateral abduction. HDsEMGs were recorded from the four muscles and analysed at both the global activation and motor unit levels. Global activation was quantified using root-mean-square (RMS) amplitude and topographic maps. Moreover, HDsEMGs were decomposed into individual motor unit spike trains and motor unit behaviour was characterized by mean discharge rate, coefficient of variation of inter-spike interval, and spatial distribution of motor unit action potentials (MUAPs). RMS maps revealed movement-specific activation within and between muscles, with the deltoid and trapezius active across all tasks, while the pectoralis and latissimus dorsi were predominantly activated during flexion and extension. Motor unit discharge rates also showed task-dependent recruitment. MUAP spatial distributions further showed distinct motor unit territories within arrays, suggesting region-specific recruitment strategies across movements. In conclusion, this framework demonstrates that individual motor unit activity can be reliably measured non-invasively in the main superficial shoulder muscles. The approach provides a methodological basis for incorporating neural control into biomechanical models of shoulder function.

Keywords: motor unit discharge rate, HDsEMG spatial distribution, neural control, shoulder biomechanics.

1.0 INTRODUCTION

Movement of the humerus requires the complex activation of the muscles of the glenohumeral joint to contract and, ultimately, cause the desired action. During these movements, the activation of large muscles such as the *trapezius, pectoralis, latissimus dorsi,* and *deltoid* must be precisely coordinated with several smaller muscles to generate torque across multiple joints and adapt to changes in both task demands and musculoskeletal alterations. According to Hughes and colleagues (1999), the muscles of the glenohumeral joint (from here on to be referred to as shoulder throughout) and their strength are an important part of functional capacity. Thus, understanding the neuromuscular behaviours of these muscles is essential for the complete understanding of this muscle group which can be used for the prescription of appropriate training and rehabilitation strategies. Biomechanical modelling of the shoulder relies on simple mechanical analysis of the body segments and the internal and external forces acting on the joint to predict the control of the muscles of the shoulder (Hughes & An, 1997; Chang *et al.*, 2000; Dickerson *et al.*, 2008). However, to date, there are restrictions to modelling advances in the shoulder, particularly due to limitations in neural control investigations of the active muscles. Specifically, these limitations stem from the methodological approach of bipolar surface electromyogram recordings to infer the intricate behaviour of the individual motor units involved in muscle activation. Additionally, to date, the addition of motoneuron behaviour from the muscles of the shoulder remains elusive (Hughes & An, 1997). Therefore, shoulder models must rely on the indirect measurement of neural control through the measurement of metrics which has been proven to be ineffective in measuring motor unit behaviour (Farina *et al.*, 2010*a*).

Classically, the approach to assessing the neural control has been through global bipolar electromyography (EMG), using amplitude measures to infer neuromuscular adaptations to specific movements with applications in biomechanics (Lawrence & De Luca, 1983; Woods

87 & Bigland-Ritchie, 1983; Hermans *et al.*, 1999; Day & Hulliger, 2001; Karlsson & Gerdle,
88 2001; Keenan *et al.*, 2005; Farina *et al.*, 2010*b*). However, the specificity of the information
89 gained from the application of the amplitude of EMG activity, in terms of inferring neural drive
90 to the muscle, is subject to debate (Farina *et al.*, 2010*b*). Waveform cancellation is particularly
91 a key factor affecting the relationship between EMG amplitude and neural drive (Yao *et al.*,
92 2000; Day & Hulliger, 2001; Dimitrova & Dimitrov, 2003; Keenan *et al.*, 2005), because as
93 additional motor units may be recruited during the gradation of force, the superposition of
94 positive and negative phases of action potentials could result in little to no increase in EMG
95 amplitude (Day & Hulliger, 2001; Keenan *et al.*, 2005). Additionally, bipolar EMG provides
96 only muscle activity in the area closest to the small electrode (i.e., local information). In the
97 case of the shoulder where large muscles produce complex movements in multiple degrees-of-
98 freedom, it is possible that not all muscle areas are active throughout all movements (i.e.,
99 within-muscle localized activation). For instance, previous evidence suggested that localized
100 regions of the deltoid, pectoralis major and latissimus dorsi can be activated based on the
101 specific shoulder movement direction (Wickham & Brown, 1998, 2012; Brown *et al.*, 2007).

102 The early 1980's advancements in myoelectric recordings have led to high-density
103 surface electromyograms (HDsEMG) (Masuda *et al.*, 1983, 1985; Reucher *et al.*, 1987;
104 Merletti *et al.*, 1999). The benefit to recording with the evolving HDsEMG technology is its
105 non-invasive nature and the ability to provide the spatial distribution of activation within and
106 across muscles during complex movements. Additionally, when combined with motor unit
107 decomposition algorithms (Holobar & Zazula, 2007; Ning *et al.*, 2015; Chen & Zhou, 2016;
108 Negro *et al.*, 2016), this approach has the potential to record a large number of concurrently
109 discharging motoneurons during voluntary contractions (Inglis *et al.*, 2025). As the alpha
110 motoneuron is the final common pathway of the neuromuscular system integrating the synaptic
111 inputs from spinal and supraspinal pathways (Liddell & Sherrington, 1925; Sherrington, 1925),

112 the analysis of the discharge behaviour of motor units provides an effective way to assemble
113 information regarding the generation and control of movement. A recent systematic review and
114 meta-analysis revealed that most motor unit behaviour investigations focused on the lower-
115 compared to upper-body which has led to a paucity of data on the upper limb (Inglis *et al.*,
116 2025). Additionally, it was revealed that of the upper limb muscles, specifically major movers
117 of the shoulder, there are few motor unit behaviour studies investigating the *upper trapezius*
118 (Westgaard & De Luca, 2001; Falla & Farina, 2008*a*, 2008*b*; Gerdle *et al.*, 2008; Holobar *et*
119 *al.*, 2009; Dideriksen *et al.*, 2016; Kirk *et al.*, 2019) and *clavicular pectoralis* (Lulic-Kuryllo
120 *et al.*, 2021*b*) using invasive or non-invasive techniques, none that examine the *latissimus dorsi*
121 (Padovan *et al.*, 2024) and only three examining the *deltoid* (de Luca *et al.*, 1982; Doherty &
122 Stashuk, 2003; Baslo *et al.*, 2024) all which are done with intramuscular means.

123 Therefore, the aim of this paper was to develop a methodological framework to
124 investigate four isometric shoulder actions (abduction, adduction, flexion and extension) at two
125 shoulder angles to fully assess the neural control of the main superficial shoulder muscles
126 (deltoid, pectoralis major, trapezius and latissimus dorsi) both at the global activation level
127 (signal amplitude) and at the motor unit level (discharge patterns). For this, we developed a
128 framework combining 6-degree-of-freedom load cell attached to an industrial robotic arm
129 while recording EMGs through the evolving HDsEMG technology. Additionally, this paper
130 provides several examples of the type of neural information of shoulder control that can be
131 extracted within the proposed framework. The novel framework proposed here will lead to the
132 establishment of guidelines for future investigations on the shoulder complex and serve to
133 propel shoulder modelling forward in these muscles.

134 **2.0 METHODS**

135 ***2.1 Participants***

136 Six healthy individuals free of any musculoskeletal or neuromuscular abnormalities (1
137 female; mean ± SD: age 28 ± 4 years; height 180 ± 7 cm; mass 79 ± 9 kg) volunteered to
138 participate in this study. All participants provided written informed consent before starting the
139 experiments that conformed to the standards set by the latest version of the Declaration of
140 Helsinki which was approved by the ethics committee of the Università degli Studi di Brescia
141 (code NP5890).

142 ***2.2 Experimental protocol***

143 *2.2.1 Experimental setup*

144 Each participant visited the lab on a single day where, in a randomized order, they
145 performed multiple degree-of-freedom isometric contractions of the shoulder in a 2-hour
146 session. Participants were seated in a rigid testing chair with their hip and knee joints at 90° of
147 flexion (0° indicates full extension) and a broad Velcro® strap placed around the midsection
148 to minimize lateral torso movements. The participant's arm was placed slightly (<20°) in the
149 scapular plane to avoid discomfort when performing the selected movements. For the
150 movements, the participants' upper arm was placed into a custom-build testing jig
151 manufactured from rectangular metal tubing to ensure a rigid transfer of forces produced to the
152 load cell (**Figure 1b**). The testing jig was attached to a 6-degrees of freedom load cell (© 2025
153 Advanced Mechanical Technology Inc., Watertown MA, USA, model #MC3A) to measure
154 force output (**Figure 1c**). The load cell has a capacity of F_x, F_y of 225 N and F_z of 445 N and a
155 sensitivity of F_x, F_y of 5.4 μV/V-N and F_z of 1.35 μV/V-N. The load cell was attached to a
156 robotic arm (Kawasaki Robotics Inc., Wixom MI, USA; **Figure 1a**) with a custom machined
157 aluminium coupling (**Figure 1d**). The importance of implementing the use of the robotic arm
158 was to position the testing jig and loadcell through fine adjustments to accommodate individual
159 anatomical landmarks to ensure participants performed each movement in the identical relative
160 position to record with precision the forces produced during each movement.

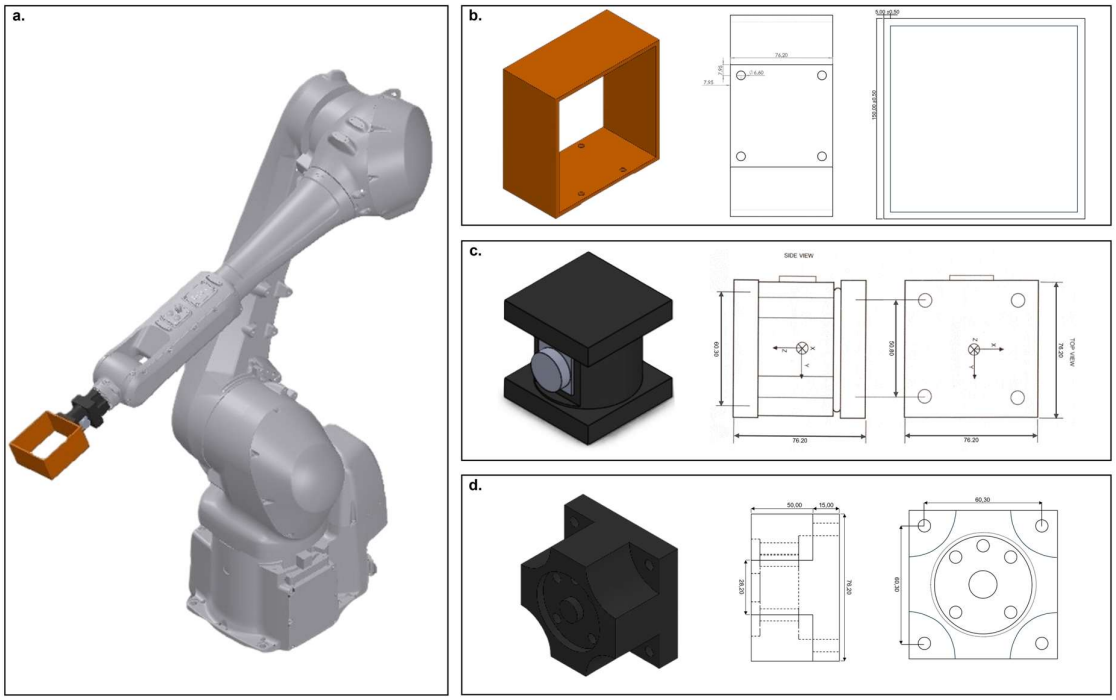

Figure 1. Mechanical components designed and manufactured for the robotic setup *(a) Complete robot assembly showing the robot with all components mounted. (b) 3D model and 2D technical drawings of the jig. (c) 3D model and 2D technical drawings of the six degree-of-freedom load cell. (d) 3D model and 2D technical drawings of the coupling between the robotic arm and the load cell. Measurements are reported in millimeters (mm).*

2.2.2 Experimental tasks

Each participant performed four isometric shoulder contractions at 30º and 65º of lateral shoulder abduction, the movements were: abduction, adduction, flexion and extension. **Figure 2** illustrates the position of the participant during the four movements across two shoulder angels. In the figure the direction of the force vector is depicted with arrows per movement. Each movement was performed at two shoulder angles to alter the deltoid muscle length (30° long; 65° short). All experimental actions were repeated twice for each movement and shoulder angle resulting in a total of 16 trials. Prior to each condition (angle/movement) participants performed three voluntary maximum isometric contractions (MVCs) for 3-5 s, with a 3-min rest between each bout. The greatest value across the three MVCs was considered as the maximal isometric shoulder force output for the individual condition and used as a reference to set the target of the submaximal contractions. Subsequently, participants underwent a short

familiarization period, during which they were instructed to exert isometric shoulder forces at 10% MVC for approximately 10 s. This familiarization task was repeated up to a maximum of five times to ensure that participants could maintain the force output as steadily as possible at a target level, which was visually assessed by a researcher. Following the familiarization period, participants were instructed to perform two isometric contractions following a trapezoidal profile. The trapezoidal pathway involved a linear increase at a rate of 3% MVC/s, a plateau phase for 30 s, and a linear decrease at a rate of 3% MVC/s. The target force output was set at 30% MVC (i.e., moderate force output) to mimic common outputs during activities of daily living (Lulic-Kuryllo *et al.*, 2021*a*).

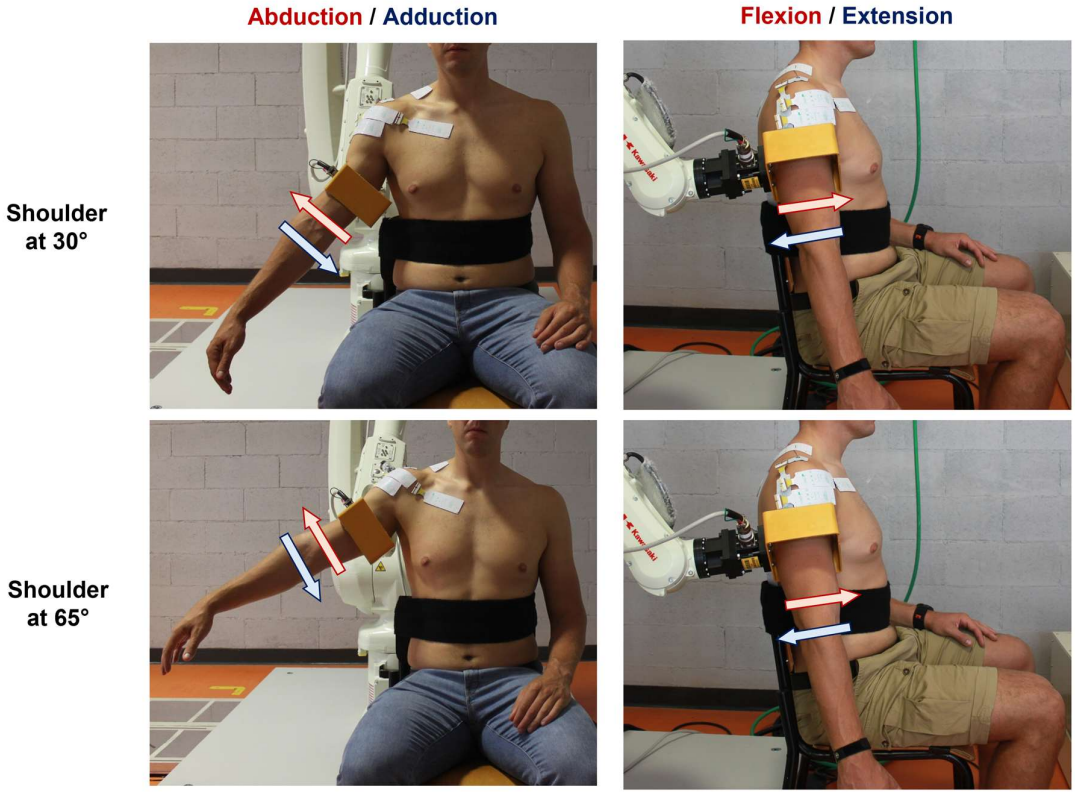

Figure 2. Experimental Movements. *Shoulder abduction/adduction (left, anterior view) and flexion/extension (right, lateral view) performed at 30° (top) and 65° (bottom) of shoulder abduction. The arm was secured to a passive robotic interface, which secured the participant in position for each given movement. A broad black Velcro® strap placed around the midsection and secured to the testing chair to minimize movements of the trunk.*

195 *2.2.3 Force feedback*

196 A novel graphical user interface (GUI) was developed in MATLAB (version 2024a) to
197 provide visual feedback of the force output and rate at which the force was to be developed
198 during the trapezoidal profile (**Figure 3e**). Force feedback was provided based on the axis
199 being investigated relative to the 3-axis load cell connected to the PC by an A-D board
200 (National Instruments CORP., NI USB-6343). The selected axis was represented by either a
201 horizontal or vertical line where the Y direction was utilized for abduction and adduction and
202 the Z direction during flexion and extension (frontal) relative to the load cell. The GUI provided
203 a green target box with the dimensions set to ± 2.5 %MVC and a blue circle to represent the
204 changes in force output. The participant was instructed to maintain the blue circle inside the
205 square. In cases where the error in force production exceeded 2.5% MVC, the square would
206 turn red, and the participant would be encouraged to meet the target force output. Visual
207 feedback was displayed on a monitor placed one meter at eye level in front of the participant.

208 ***2.3 Data collection***

209 HDsEMGs were acquired from the four major shoulder girdle movers (deltoid,
210 pectoralis major, upper trapezius and latissimus dorsi) during the submaximal isometric
211 movements using 6 two-dimensional adhesive arrays (HD08MM1305 and HD08MM1606; 1
212 mm diameter; 8 mm inter-electrode distance; OT Bioelettronica, Turin, Italy). The arrays
213 placed on the deltoid and pectoralis major (see below) consisted of 64 electrodes arranged in
214 13 rows by 5 columns, with one missing channel in the top left corner. As for the upper
215 trapezius and the latissimus dorsi, the arrays consisted of 96 electrodes arranged in 16 rows by
216 6 columns. Prior to array and ground placement, the area was shaved, mildly abraded (EVERI,
217 Spes Medica, Genova, Italy) and cleaned with distilled water. The electrode-skin contact was
218 ensured by filling the foam cavities with conductive paste (AC cream, Spes Medica, Genova,

219 Italy). Two reference electrodes were used; one positioned on the right elbow at the level of
220 the epicondyles and other on the acromion process.

221 We piloted several arrays and configurations to achieve the greatest motor unit yield in
222 the deltoid (see appendix A). For the anterior/middle deltoid, the electrode was placed
223 approximately 2 cm distal to the proximal deltoid tendon, starting from the anterior border
224 horizontally towards the posterior portion perpendicular to the insertion of the middle fibres to
225 the humerus (*array 1*, **Figure 3a**). To cover more of this anterior and middle aspect of the
226 deltoid a second array was place distally and slightly offset (2 array columns) and parallel to
227 the proximal array (*array 2*, **Figure 3a**). For the posterior deltoid, the electrode was positioned
228 in line with the posterior aspect of the deltoid adjacent to the distal deltoid array (*array 3*,
229 **Figure 3a**). For the clavicular region of the pectoralis major, the electrode was placed
230 approximately 2 cm inferior to the clavicle (superior array in (Lulic-Kuryllo *et al.*, 2021*a*);
231 *array 4*, **Figure 3b**). For the upper trapezius, the electrode array was positioned to bisect the
232 7th and 8th row (*array 5*, **Figure 3c**) along the line drawn between C7 and the lateral edge of
233 the acromion due to the use of the 96-electrode array which is larger (3 extra rows and 1 extra
234 column) than the standard 64 electrode array used in the deltoid and pectorals above (modified
235 from (Falla & Farina, 2008*b*). For the latissimus dorsi, a line was drawn approximately 3 cm
236 inferior and horizontal to the posterior axillary crease and parallel to the superior aspect of the
237 iliac crest. From these lines a diagonal line was drawn to follow the latissimus dorsi muscle
238 fibres, and the array was placed in the middle of this area ensuring that majority of the array
239 covered the bulk of the muscle (Padovan *et al.*, 2024) (*array 6*, **Figure 3d**).
240

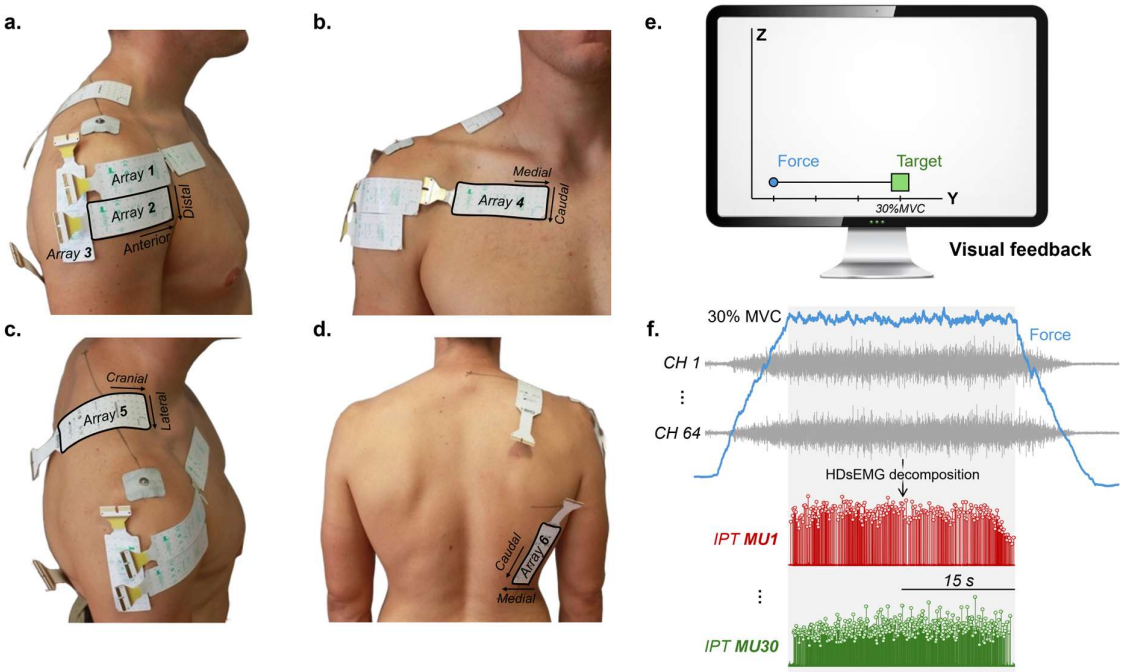

Figure 3. Electrode placement, visual feedback and HDsEMG analysis. *(a) Electrode placement for the deltoid. Array 1 was positioned horizontally approximately 2 cm distal from the insertion of the deltoid tendon. Array 2 was placed distally and slightly offset to cover the middle and anterior deltoid. Array 3 was positioned vertically adjacent to the distal deltoid array. (b) Electrode placement for the clavicular region of the pectoralis major. Array 4 was positioned horizontally and approximately 2 cm inferior to the clavicle, avoiding the sternum. (c) Electrode placement of the trapezius. Array 5 was positioned to bisect the 7th and 8th row of the array along the line between C7 and the acromion process. (d) Electrode placement of the latissimus dorsi. Array 6 was positioned diagonally in the middle of an area delimited by two horizontal lines, drawn approximately 3 cm inferior to the posterior axillary crease and parallel to the superior aspect of the iliac crest, the array was placed in line with the muscle fibers. (e) Visual feedback of the force output. Visual feedback was provided from a line, a square box and a circle representing the pathway, the target force and the force output of the participant, respectively. (f) Schematic representation of the HDsEMG decomposition. HDsEMGs were visually inspected and, subsequently, decomposed into motor unit innervation pulse train (IPTs). The 30-s plateau phase was considered for this analysis (light gray rectangle).*

HDsEMG and force outputs were digitized synchronously at a sampling frequency of 2000 Hz using a 16-bit A/D converter (10-500 Hz bandwidth; Novecento+, OT Bioelettronica, Turin, Italy). HDsEMG signals were recorded in monopolar derivation and amplified (8 V/V) to maximize signal resolution while avoiding saturation.

2.4 Data analysis

264 HDsEMG recordings were analysed offline in MATLAB (version 2024a) using
265 custom-written scripts. As potential applications of the developed experimental framework,
266 analyses were performed both at the global HDsEMG level (signal amplitude) and at the motor
267 unit level (discharge patterns) to assess the neural control of shoulder muscles. For all analyses,
268 the 30-s plateau phase of each contraction was selected. HDsEMGs were bandpass filtered
269 between 20 and 500 Hz using a third-order Butterworth filter and, after that, visually inspected
270 to identify and remove bad channels due to electrode-skin contact issues or artifacts (mean ±
271 SD: 2 ± 1 channels removed for all movements and shoulder angles).

272 *2.4.1 HDsEMG root-mean-square amplitude*

273 To assess the global activation of the investigated muscles, the root-mean-square
274 (RMS) amplitude was used. Initially, single-differential (bipolar) EMGs were calculated as
275 the algebraic difference between monopolar signals detected by consecutive rows of electrodes.
276 Then, the RMS amplitude was calculated for each of the 59 (64-electrodes array) and 80 (96-
277 electrodes array) single-differential channels using non-overlapping windows of 250 ms (Mark
278 Burden *et al.*, 2014). The average value across windows was considered for further analysis,
279 providing topographic maps of RMS amplitude for each of the investigated muscles. For
280 simplicity, only *array 2* of the deltoid was analysed. The average RMS amplitude across all
281 channels was then considered as the global RMS amplitude of the muscle for each movement
282 and shoulder angle.

283 *2.4.2 HDsEMG decomposition*

284 HDsEMG signals were completely decomposed into their constituent motor unit spike
285 trains using a convolutive blind-source separation algorithm (Negro *et al.*, 2016). Briefly, after
286 extending and whitening the HDsEMG signals, a fixed-point algorithm that seeks sources that
287 maximize a measure of sparsity was applied to identify the motor unit spike trains (**Figure 3f**).

288 The spikes were separated from the noise using the K-means algorithm and, while iteratively
289 updating the motor unit separation vectors, the discharge times estimation was further refined
290 by minimizing the coefficient of variation of the inter-spike intervals. This decomposition
291 method has been previously validated (Negro *et al.*, 2016) and extensively applied to assess
292 the activity of single motor units (Negro *et al.*, 2016; Cogliati *et al.*, 2020; Cabral *et al.*, 2024).
293 After the automatic identification of motor units, any missed or misidentified motor unit
294 discharges which produced non-physiological discharge rates (< 4 pulses per second or > 50
295 pulses per second; (Negro *et al.*, 2009) were manually identified and iteratively edited by an
296 experienced operator, and the subsequent motor unit spike trains were re-estimated (Martinez-
297 Valdes *et al.*, 2017; Hassan *et al.*, 2020). This approach has been shown to be highly reliable
298 across operators (Hug *et al.*, 2021). Only motor units with a silhouette (SIL) value, which is a
299 quality control measure of the decomposition accuracy, greater than 0.87 (Negro *et al.*, 2016)
300 (Negro *et al*., 2016) were included in the further analysis.

301 *2.4.3 Motor unit discharge behaviour*

302 The instantaneous discharge rate of each identified motor unit was determined by
303 computing the inverse of the inter-spike interval and, subsequently, the mean discharge rate
304 was calculated and considered for further analysis. Moreover, the coefficient of variation of
305 the inter-spike interval (CoV-ISI) was calculated by dividing the standard deviation of the
306 inter-spike interval by its mean.

307 *2.4.4 Motor unit action potential amplitude*

308 To assess the spatial distribution of motor unit action potentials (MUAP), templates
309 were obtained using the spike-triggered averaging technique (Stein *et al.*, 1972). Specifically,
310 single-differential EMGs were segmented into 100-ms windows centred on the discharge times
311 of individual motor units and averaged. The peak-to-peak amplitude of each template was then

calculated across channels, generating topographical MUAP amplitude maps. These maps were used both to validate the decomposed motor units and to exemplify the type of neural information that can be extracted with the proposed framework. As for the HDsEMG RMS amplitude analysis, only *array 2* of the deltoid was analysed. As an additional example analysis, the centroid of the deltoid MUAPs was calculated from active channels, defined as those with a peak-to-peak amplitude greater than 70% of the maximum observed across the grid (Vieira *et al.*, 2010), and compared across movements.

2.5 Statistical analysis

All statistical analyses were performed in R (version 4.2.2), using the RStudio environment. Linear mixed-effect models (LMM) were applied for all statistical analyses, as they account for the non-independence of data points within each participant, which is particularly relevant for motor unit data. To compare global RMS amplitude, mean discharge rate and CoV-ISI, random intercept models were applied with movement (abduction, adduction, flexion and extension) and muscle (deltoid, pectoralis, trapezius and latissimus dorsi) as the fixed effects and participant as the random effect (e.g., *mean discharge rate ~ 1 + movement*muscle + (1 | participant)*). LMMs were implemented using the package *lmerTest* (Kuznetsova *et al.*, 2017) with the Kenward-Roger method to approximate the degrees of freedom and estimate the *p*-values. The *emmeans* package was used, when necessary, for multiple comparisons and to determine estimated marginal means with 95% confidence intervals (Lenth *et al.*, 2019).

3.0 RESULTS

3.1 HDsEMG root-mean-square amplitude

Figure 4a depicts the topographical maps of RMS amplitude at 30° shoulder angle across muscle and movements for a selected participant. During abduction, the deltoid is the

most active muscle, particularly in the central-anterior portion of the *array 2* (see **Figure 3a**), followed by the caudal area of the trapezius. As for the pectoralis and latissimus dorsi, during abduction there is no visual evidence of significant activation. During adduction, most of the activity is in the latissimus dorsi covering much of the array, followed by a small amount of activity in the medial-caudal part of the array in the pectoralis. There is no evident activity in the deltoid and trapezius during adduction. During flexion, most of the activity is in the deltoid anterior region, followed by the pectoralis. During extension, the deltoid was again the most active, but towards the posterior aspect of the array. There was also significant activity in the caudal region of the array in the latissimus dorsi and the trapezius, with no evident activity in the pectoralis. In **Figure 4b,** the topographical RMS amplitude maps for the same selected participants are depicted but at 65° shoulder angle. The activation patterns during abduction, adduction, and flexion closely resembled those reported above for the 30° condition During extension, the deltoid was very active across *array 2*. Additionally, as seen for the 30° condition, a significant amount of activity was observed in the caudal region of the trapezius, but with little activity in the latissimus dorsi.

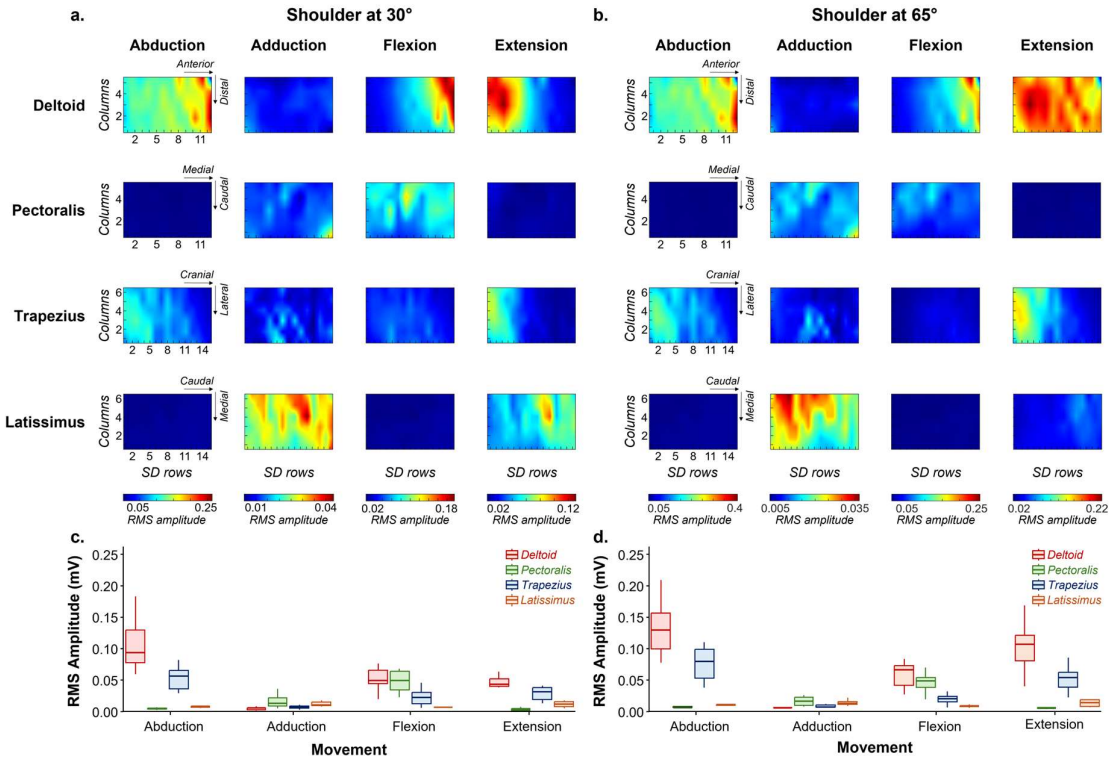

Figure 4. Muscle activation patterns across shoulder movements at 30° and 65°. *RMS amplitude topographical maps for the deltoid, pectoralis major, trapezius, and latissimus dorsi during abduction, adduction, flexion and extension. These movements were performed with the shoulder positioned at 30° of lateral abduction (a) and 65° (b). The x- and y-axes represent the rows and columns of the array, with color intensity (from dark blue to dark red) indicating the level of muscle excitation. (c and d) Group results of the RMS amplitude for each movement and muscle. Horizontal traces, boxes, and whiskers represent the median value, interquartile interval, and distribution range, respectively.*

Figure 4c shows the group results for the global RMS amplitude at 30° shoulder angle. There was a statistically significant interaction between muscle and movement (LMM, F=32.911, p<0.001). For the abduction, the deltoid muscle presented significantly higher global RMS amplitude compared to all the other muscles (p<0.001 for all comparisons). Additionally, trapezius RMS amplitude was significantly greater than pectoralis and latissimus RMS amplitude (p<0.001 for both comparisons). For the adduction, no significant differences were observed across all muscles (p>0.634 for all comparisons). For the flexion, the RMS amplitude of the deltoid and pectoralis major muscles was significantly greater than the trapezius and latissimus dorsi (p<0.031 for all comparisons). Finally, for the extension, the

deltoid muscle presented a higher RMS amplitude compared to the pectoralis major and latissimus dorsi ($p<0.041$ for both comparisons), with no other significant differences across muscles ($p>0.069$).

Similar results were observed at 65° shoulder angle (**Figure 4d**), where there was a statistically significant muscle*movement interaction (LMM, $F=33.903$, $p<0.001$). For the abduction, the deltoid muscle presented greater RMS amplitude compared to all the other muscles ($p<0.001$ for all comparisons). Furthermore, trapezius RMS amplitude was significantly higher than pectoralis and latissimus ($p<0.001$ for both comparisons). For the adduction, no significant differences were observed across muscles ($p>0.808$ for all comparisons). For the flexion, the global RMS amplitude of the deltoid muscle was significantly greater compared to the trapezius and latissimus dorsi ($p<0.003$ for both comparisons). In addition, the pectoralis major muscle showed a higher RMS amplitude than the latissimus dorsi ($p=0.004$). For the extension, the RMS amplitude of the deltoid muscle was significantly greater compared to all the other muscles ($p<0.001$ for all comparisons). Additionally, the trapezius RMS amplitude was greater than the pectoralis major and latissimus dorsi ($p<0.004$ for both comparisons).

3.2 Motor unit discharge behaviour

Figure 5 and **Figure 6** illustrate, for different shoulder movements at a 30° shoulder angle, the neural features at the motor unit level that can be extracted using the proposed framework. For each muscle, representative MUAP amplitude maps and the corresponding motor unit instantaneous discharge rates are presented. During abduction (**Figure 5**), motor units could be identified only in the deltoid and trapezius muscles for this representative participant, with 30 and 19 units decomposed, respectively. In the deltoid, motor units were distributed across different regions of the array, including anterior (MUAP 1 and MUAP 30),

central (MUAP 3 and MUAP 5), and posterior regions (MUAP 2 and MUAP 4). In contrast, most trapezius motor units were located cranially within the array. Additionally, most motor units from both muscles were tonically active throughout the plateau phase of the task.

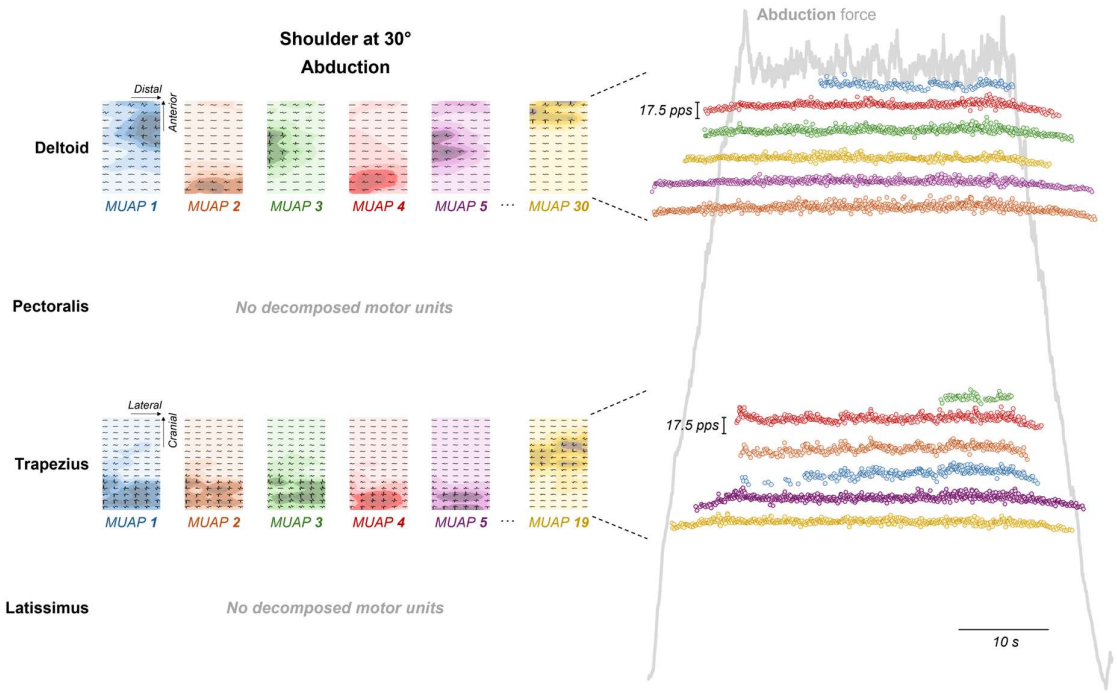

Figure 5: Motor unit action potential amplitude maps and motor unit discharge rates during shoulder abduction at 30° *Motor unit action potentials were obtained using the spike-triggered averaging technique. For this representative subject, motor units were identified in the deltoid (30 units) and trapezius (19 units). No motor units were decomposed from the pectoralis or latissimus dorsi (left panel). Abduction force profile (gray line), and motor unit instantaneous discharge rates are shown in the right panel. Separately per muscle, each motor unit is represented with a color, used both for the MUAP distribution maps and the instantaneous discharge rates.*

Figure 6 shows the same representative participant during the flexion movement. In this condition, identifiable motor units were found in the deltoid (20 units), pectoralis (21 units), and trapezius (16 units), whereas no motor units were identified in the latissimus dorsi. Deltoid motor units were predominantly located in the anterior region of the array (e.g., MUAP 1, MUAP 2, and MUAP 5). For both the trapezius and pectoralis, motor units were distributed across different regions of their respective arrays. While most deltoid and pectoralis motor

units were tonically active throughout the plateau phase, some trapezius units exhibited more intermittent activity.

Table 1 summarizes the motor unit yield across all muscles, movements, and shoulder angles. Overall, a higher number of motor units were decomposed at the 30° shoulder angle compared with 65°. Consistent with the representative case, no motor units were identified in the pectoralis major and latissimus dorsi during abduction, or in the latissimus dorsi during flexion. In addition, no units were decomposed from the pectoralis during extension.

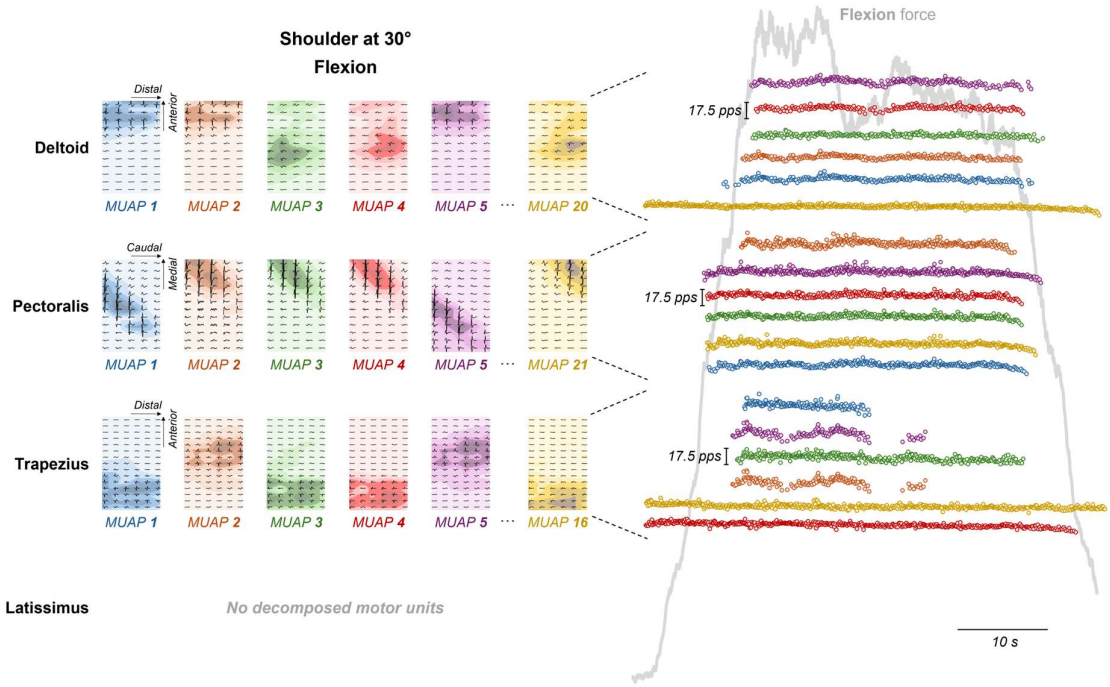

Figure 6: Motor unit action potential amplitude maps and motor unit discharge rates during shoulder flexion at 30°. *Motor unit action potentials were obtained using the spike-triggered averaging technique. For this representative subject (same as in Figure 5), motor units were decomposed from the deltoid (20 units), pectoralis (21 units), and trapezius (16 units). No motor units were decomposed from the latissimus dorsi (left panel). Flexion force profile (gray line), and motor unit instantaneous discharge rates are shown in the right panel. Separately per muscle, each motor unit is represented with a color, used both for the MUAP distribution maps and the instantaneous discharge rates.*

Table 1: *Average ± standard deviation motor unit yield across all muscles (deltoid, pectoralis, trapezius and latissimus), movements (abduction, adduction, flexion and extension) and shoulder angles (30° or 65°).*

	SHOULDER AT 30 DEGREES				SHOULDER AT 65 DEGREES			
	Abduction	**Adduction**	**Flexion**	**Extension**	**Abduction**	**Adduction**	**Flexion**	**Extension**
Deltoid	12 ± 19	9 ± 15	10 ± 11	12 ± 7	7 ± 7	2 ± 3	10 ± 9	10 ± 11

Pectoralis	0 ± 0	5 ± 3	5 ± 7	0 ± 0	0 ± 0	6 ± 6	5 ± 6	0 ± 0
Trapezius	6 ± 6	5 ± 9	5 ± 5	5 ± 4	5 ± 3	3 ± 1	5 ± 2	4 ± 2
Latissimus	0 ± 0	5 ± 5	0 ± 0	3 ± 3	0 ± 0	3 ± 4	0 ± 0	2 ± 2

Figure 7 shows the group results for motor unit mean discharge rate (top) and CoV-ISI (bottom). For the 30° shoulder angle (**Figure 7a**), there was a statistically significant interaction between muscle and movement (LMM, F=3.190, p=0.008). For the abduction, there was no significant differences between the mean discharge rate of deltoid and trapezius motor units (p=0.282). Similarly, for the adduction, no significant differences in motor unit mean discharge rate were observed across muscles (p>0.058 for all comparisons). For the flexion, the pectoralis major motor units presented significantly greater mean discharge rates compared to both trapezius and deltoid motor units (p<0.044 for both comparisons). For the extension, both the deltoid and trapezius motor units showed significantly higher discharge rates than the latissimus dorsi motor units (p<0.005 for both comparison), with no significant differences between them (p=0.969). Similarly, for the 65° shoulder angle (**Figure 7b**), there was a significant muscle*movement interaction (LMM, F=6.821, p<0.001). For the abduction, no significant differences were found in the mean discharge rate of the deltoid and trapezius motor units (p=0.308). For the adduction, significant higher discharge rates were found for trapezius compared to deltoid motor units (p<0.013). For the flexion, both the deltoid and pectoralis major motor units showed higher discharge rates than the trapezius (p<0.001 for both comparisons), while no significant differences were observed between deltoid and pectoralis major motor units (p=0.537). For the extension, deltoid and trapezius motor units presented significantly greater mean discharge rates compared to the latissimus dorsi (p<0.017), with no significant differences between them (p=0.311).

When examining the variability of the motor unit discharge rate (CoV-ISI), for the 30° shoulder angle (**Figure 7c**), there was a statistically significant interaction between muscle and

movement (LMM, F=3.037, p=0.010). For the abduction, the trapezius presented a higher CoV-ISI compared to the deltoid muscle (p=0.009). Similarly, for the adduction, the trapezius CoV-ISI was significantly higher than the pectoralis major and latissimus dorsi motor units (p<0.001 for both comparisons), with no other significant differences across muscles (p>0.262 for all comparisons). For the flexion, the trapezius motor units showed significantly greater CoV-ISI compared to both the deltoid and pectoralis major (p<0.002). For the extension, no significant differences in CoV-ISI were observed across muscles (p>0.060). For the 65° shoulder angle (**Figure 7d**), there was also a significantly muscle*movement interaction (LMM, F=4.437, p<0.001). For the abduction, no significant differences in the CoV-ISI were observed between the deltoid and trapezius motor units (p=0.215). For the adduction, the CoV-ISI of deltoid motor units was significantly greater than the pectoralis major and latissimus dorsi motor units (p<0.021), with no other significant differences across muscles (p>0.110). For the flexion, the trapezius motor units presented significantly greater CoV-ISI values compared to the pectoralis major (p<0.017). For the extension, the latissimus dorsi motor units showed significantly greater CoV-ISI values than both the deltoid and trapezius (p<0.010).

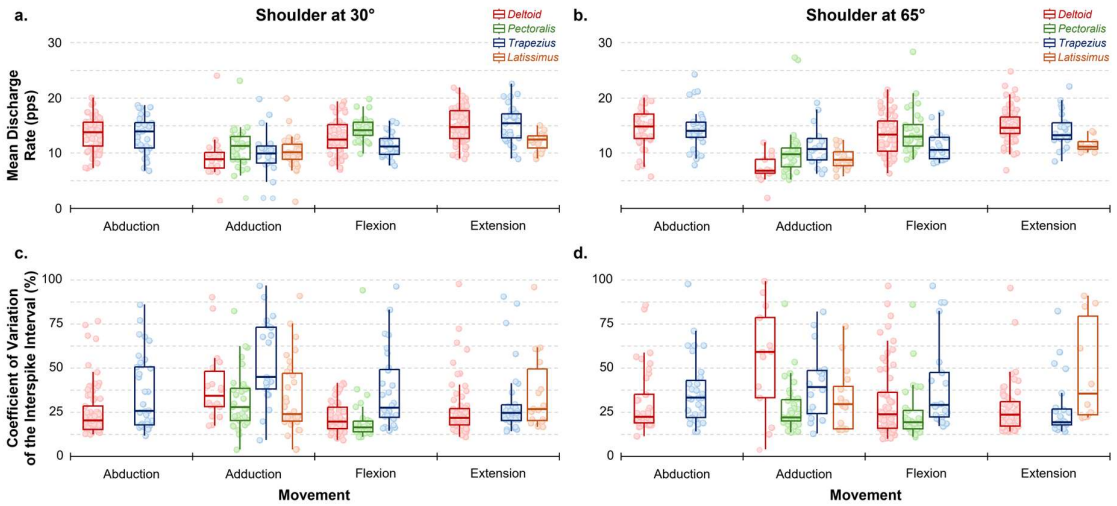

***Figure 7: Motor unit discharge behavior across movements and elevation angle**. Group results for the motor unit mean discharge rate (a and b) and the CoV-ISI (c and d) during abduction, adduction, flexion, and extension at both 30° (left) and 65° (right) shoulder angles.*

Horizontal traces, boxes, and whiskers represent the median value, interquartile interval, and distribution range, respectively; individual circles correspond to single motor units.

4.0 DISCUSSION

The goal of this methodological paper was to investigate four isometric shoulder movements at two angles to fully assess the neural control of the main superficial shoulder muscles (deltoid, pectoralis major, trapezius and latissimus dorsi) at both the global EMG level (RMS amplitude) and at the motor unit level (discharge patterns). To our knowledge, this is the first to record motor unit behaviour with non-invasive HDsEMG in the deltoid and latissimus dorsi. The proposed framework demonstrates the feasibility of integrating global and motor unit analyses to advance the understanding of shoulder muscle control and provides a foundation for improving biomechanical modelling of the shoulder.

The RMS topographical maps showed distinct activation patterns across muscles and movements. As expected, the deltoid was the primary contributor during abduction, while the pectoralis major and latissimus dorsi were mainly active during flexion and extension/adduction, respectively. The trapezius displayed consistent activation across conditions, reflecting its role in stabilizing the shoulder during multi-directional force generation. Importantly, only minor changes in spatial activation patterns were observed between 30° and 65° of abduction, although deltoid activity was moderately greater at the shorted muscle length (see **Figure 4**). These findings align with previous evidence that localized muscle regions can be selectively recruited depending on shoulder movement direction (Wickham & Brown, 1998, 2012; Brown *et al.*, 2007). They also highlight the limitation of relying solely on RMS amplitude from bipolar EMG, which, due to waveform cancellation, may not fully capture underlying neural activity (Day & Hulliger, 2001; Keenan *et al.*, 2005).

The analysis of decomposed motor unit discharge behaviour (**Figure 7**) generally mirrored the RMS amplitude trends but provided a more detailed view of neural control. For instance, during abduction, motor units were identified only in the deltoid and trapezius, with similar discharge rates, supporting their dominant role in this task. Conversely, during flexion, deltoid and pectoralis major motor units exhibited comparable mean discharge rates, whereas trapezius motor units discharged at significantly lower rates, suggesting a more stabilizing than prime-mover contribution. These examples illustrate how motor unit analyses may be more sensitive than global EMG in detecting subtle differences in task-specific muscle contributions.

The spatial distribution of MUAPs further demonstrated movement-specific recruitment. Although motor units were not tracked across tasks, differences in the sets of active units between abduction and flexion strongly suggest task-dependent recruitment and de-recruitment, consistent with previous findings in other upper-limb muscles (ter Haar Romeny *et al.*, 1984). This capability of the framework to map motor unit territories and discharge patterns (**Figure 5** and **Figure 6**) provides a novel tool for probing the neural strategies underlying complex shoulder control.

A notable observation was the large variability in motor unit discharge rate variability (CoV-ISI), particularly at the 65° shoulder angle. Higher discharge variability may reflect increased task complexity and the greater need for synergistic adjustments between muscles to maintain stable force output (Calvin & Stevens, 1968). However, further research is warranted to clarify how discharge variability changes with contraction intensity and in multiple degrees-of-freedom tasks.

5.0 LIMITATIONS

Despite the rigor taken to control the specific shoulder movements and position, several limitations should be acknowledged. First, although participants were stabilized with straps

522 and a rigid jig, the inherent flexibility of the shoulder joint may have introduced small
523 variations in movement execution. While this may reduce experimental control, it also
524 increases ecological validity by better replicating strategies used in daily activities. Second,
525 only two joint angles within the mid-range were tested, limiting extrapolation to positions
526 closer to 0° or 180°. Third, contractions were restricted to 30% MVC, chosen to reflect
527 moderate force demands of daily living, but additional work is needed across lower and higher
528 force levels. Fourth, the sample included only one female participant, precluding sex
529 comparisons. Finally, only four major superficial shoulder muscles were recorded. The
530 inability to assess particularly the scapular stabilizers is a key omission given their likely
531 contribution during extension and adduction tasks.

532 **6.0 CONCLUSIONS**

533 The present study demonstrates that it is feasible to record and analyse motor unit
534 behaviour of major shoulder muscles using HDsEMG during controlled isometric tasks. The
535 framework combines global EMG and motor unit analyses with precise force measurements to
536 provide complementary insights into both muscle-level activation and neural control strategies.
537 These methodological advances are essential for the development of comprehensive
538 biomechanical models of the shoulder that incorporate not only anatomical and mechanical
539 properties but also neural control mechanisms.

REFERENCES

Baslo SA, Şirin NG, Orhan EK, Baslo MB & Öge AE (2024). Selective Muscle Involvement in Amyotrophic Lateral Sclerosis: Evidence Inferred from the Point of Motor Unit Firing Rates. *Noro Psikiyatr Ars* **61,** 296–305.

Brown JMM, Wickham JB, McAndrew DJ & Huang X-F (2007). Muscles within muscles: Coordination of 19 muscle segments within three shoulder muscles during isometric motor tasks. *J Electromyogr Kinesiol* **17,** 57–73.

Cabral HV, Inglis JG, Cudicio A, Cogliati M, Orizio C, Yavuz US & Negro F (2024). Muscle contractile properties directly influence shared synaptic inputs to spinal motor neurons. *The Journal of Physiology*; DOI: 10.1113/JP286078.

Calvin WH & Stevens CF (1968). Synaptic noise and other sources of randomness in motoneuron interspike intervals. *Journal of Neurophysiology* **31,** 574–587.

Chang YW, Hughes RE, Su FC, Itoi E & An KN (2000). Prediction of muscle force involved in shoulder internal rotation. *J Shoulder Elbow Surg* **9,** 188–195.

Chen M & Zhou P (2016). A Novel Framework Based on FastICA for High Density Surface EMG Decomposition. *IEEE Transactions on Neural Systems and Rehabilitation Engineering* **24,** 117–127.

Cogliati M, Cudicio A, Martinez-Valdes E, Tarperi C, Schena F, Orizio C & Negro F (2020). Half marathon induces changes in central control and peripheral properties of individual motor units in master athletes. *J Electromyogr Kinesiol* **55,** 102472.

Day SJ & Hulliger M (2001). Experimental simulation of cat electromyogram: evidence for algebraic summation of motor-unit action-potential trains. *Journal of Neurophysiology* **86,** 2144–2158.

Dickerson CR, Hughes RE & Chaffin DB (2008). Experimental evaluation of a computational shoulder musculoskeletal model. *Clin Biomech (Bristol)* **23,** 886–894.

Dideriksen JL, Holobar A & Falla D (2016). Preferential distribution of nociceptive input to motoneurons with muscle units in the cranial portion of the upper trapezius muscle. *Journal of Neurophysiology* **116,** 611–618.

Dimitrova NA & Dimitrov GV (2003). Interpretation of EMG changes with fatigue: facts, pitfalls, and fallacies. *J Electromyogr Kinesiol* **13,** 13–36.

Doherty TJ & Stashuk DW (2003). Decomposition-based quantitative electromyography: Methods and initial normative data in five muscles. *Muscle Nerve* **28,** 204–211.

Falla D & Farina D (2008*a*). Motor units in cranial and caudal regions of the upper trapezius muscle have different discharge rates during brief static contractions. *Acta Physiologica* **192,** 551–558.

Falla D & Farina D (2008*b*). Non-uniform adaptation of motor unit discharge rates during sustained static contraction of the upper trapezius muscle. *Exp Brain Res* **191,** 363–370.

578 Farina D, Holobar A, Merletti R & Enoka RM (2010*a*). Decoding the neural drive to muscles
579 from the surface electromyogram. *Clinical Neurophysiology* **121,** 1616–1623.

580 Farina D, Holobar A, Merletti R & Enoka RM (2010*b*). Decoding the neural drive to muscles
581 from the surface electromyogram. *Clinical Neurophysiology* **121,** 1616–1623.

582 Gerdle B, Östlund N, Grönlund C, Roeleveld K & Karlsson JS (2008). Firing rate and
583 conduction velocity of single motor units in the trapezius muscle in fibromyalgia
584 patients and healthy controls. *Journal of Electromyography and Kinesiology* **18,** 707–
585 716.

586 ter Haar Romeny BM, van der Gon JJ & Gielen CC (1984). Relation between location of a
587 motor unit in the human biceps brachii and its critical firing levels for different tasks.
588 *Exp Neurol* **85,** 631–650.

589 Hassan A, Thompson CK, Negro F, Cummings M, Powers RK, Heckman CJ, Dewald JPA &
590 McPherson LM (2020). Impact of parameter selection on estimates of motoneuron
591 excitability using paired motor unit analysis. *J Neural Eng* **17,** 016063.

592 Hermans V, Spaepen AJ & Wouters M (1999). Relation between differences in
593 electromyographic adaptations during static contractions and the muscle function.
594 *Journal of Electromyography and Kinesiology* **9,** 253–261.

595 Holobar A, Farina D, Gazzoni M, Merletti R & Zazula D (2009). Estimating motor unit
596 discharge patterns from high-density surface electromyogram. *Clin Neurophysiol* **120,**
597 551–562.

598 Holobar A & Zazula D (2007). Multichannel Blind Source Separation Using Convolution
599 Kernel Compensation. *IEEE Transactions on Signal Processing* **55,** 4487–4496.

600 Hug F, Avrillon S, Del Vecchio A, Casolo A, Ibanez J, Nuccio S, Rossato J, Holobar A &
601 Farina D (2021). Analysis of motor unit spike trains estimated from high-density
602 surface electromyography is highly reliable across operators. *J Electromyogr*
603 *Kinesiol*102548.

604 Hughes RE & An K-N (1997). Monte Carlo simulation of a planar shoulder model. *Med Biol*
605 *Eng Comput* **35,** 544–548.

606 Hughes RE, Johnson ME, O'Driscoll SW & An K-N (1999). Age-Related Changes in
607 Normal Isometric Shoulder Strength. *Am J Sports Med* **27,** 651–657.

608 Inglis JG, Cabral HV, Cosentino C, Bonardi A & Negro F (2025). Motor unit discharge
609 behavior in human muscles throughout force gradation: a systematic review and meta-
610 analysis with meta-regression. *Journal of Applied Physiology* **138,** 1050–1065.

611 Karlsson S & Gerdle B (2001). Mean frequency and signal amplitude of the surface EMG of
612 the quadriceps muscles increase with increasing torque — a study using the
613 continuous wavelet transform. *Journal of Electromyography and Kinesiology* **11,**
614 131–140.

Keenan KG, Farina D, Maluf KS, Merletti R & Enoka RM (2005). Influence of amplitude cancellation on the simulated surface electromyogram. *Journal of Applied Physiology* **98,** 120–131.

Kirk EA, Gilmore KJ, Stashuk DW, Doherty TJ & Rice CL (2019). Human motor unit characteristics of the superior trapezius muscle with age-related comparisons. *Journal of Neurophysiology* **122,** 823–832.

Kuznetsova A, Brockhoff PB & Christensen RHB (2017). lmerTest Package: Tests in Linear Mixed Effects Models. *J Stat Soft* **82,** 1–26.

Lawrence JH & De Luca CJ (1983). Myoelectric signal versus force relationship in different human muscles. *Journal of Applied Physiology* **54,** 1653–1659.

Lenth RV, Bolker B, Buerkner P, Giné-Vázquez I, Herve M, Jung M, Love J, Miguez F, Piaskowski J, Riebl H & Singmann H (2019). emmeans. Available at: https://cran.r-project.org/web/packages/emmeans/index.html [Accessed September 19, 2024].

Liddell EGT & Sherrington CS (1925). Recruitment and some other features of reflex inhibition. *Proceedings of the Royal Society of London Series B, Containing Papers of a Biological Character* **97,** 488–518.

de Luca CJ, LeFever RS, McCue MP & Xenakis AP (1982). Behaviour of human motor units in different muscles during linearly varying contractions. *The Journal of Physiology* **329,** 113–128.

Lulic-Kuryllo T, Negro F, Jiang N & Dickerson CR (2021*a*). Standard bipolar surface EMG estimations mischaracterize pectoralis major activity in commonly performed tasks. *Journal of Electromyography and Kinesiology* **56,** 102509.

Lulic-Kuryllo T, Thompson CK, Jiang N, Negro F & Dickerson CR (2021*b*). Neural control of the healthy pectoralis major from low-to-moderate isometric contractions. *J Neurophysiol* **126,** 213–226.

Mark Burden A, Lewis SE & Willcox E (2014). The effect of manipulating root mean square window length and overlap on reliability, inter-individual variability, statistical significance and clinical relevance of electromyograms. *Manual Therapy* **19,** 595–601.

Martinez-Valdes E, Negro F, Laine CM, Falla D, Mayer F & Farina D (2017). Tracking motor units longitudinally across experimental sessions with high-density surface electromyography. *J Physiol* **595,** 1479–1496.

Masuda T, Miyano H & Sadoyama T (1983). The propagation of motor unit action potential and the location of neuromuscular junction investigated by surface electrode arrays. *Electroencephalography and Clinical Neurophysiology* **55,** 594–600.

Masuda T, Miyano H & Sadoyama T (1985). A surface electrode array for detecting action potential trains of single motor units. *Electroencephalogr Clin Neurophysiol* **60,** 435–443.

Merletti R, Farina D & Granata A (1999). Non-invasive assessment of motor unit properties with linear electrode arrays. *Electroencephalogr Clin Neurophysiol Suppl* **50,** 293–300.

Negro F, Holobar A & Farina D (2009). Fluctuations in isometric muscle force can be described by one linear projection of low-frequency components of motor unit discharge rates. *The Journal of Physiology* **587,** 5925–5938.

Negro F, Muceli S, Castronovo AM, Holobar A & Farina D (2016). Multi-channel intramuscular and surface EMG decomposition by convolutive blind source separation. *J Neural Eng* **13,** 026027.

Ning Y, Zhu X, Zhu S & Zhang Y (2015). Surface EMG Decomposition Based on K-means Clustering and Convolution Kernel Compensation. *IEEE Journal of Biomedical and Health Informatics* **19,** 471–477.

Padovan R, Toninelli N, Longo S, Tornatore G, Esposito F, Cè E & Coratella G (2024). High-Density Electromyography Excitation in Front vs. Back Lat Pull-Down Prime Movers. *J Hum Kinet* **91,** 47–60.

Reucher H, Rau G & Silny J (1987). Spatial filtering of noninvasive multielectrode EMG: Part I--Introduction to measuring technique and applications. *IEEE Trans Biomed Eng* **34,** 98–105.

Sherrington CS (1925). Remarks on some aspects of reflex inhibition. *Proceedings of the Royal Society of London Series B, Containing Papers of a Biological Character* **97,** 519–545.

Stein RB, French AS, Mannard A & Yemm R (1972). New methods for analysing motor function in man and animals. *Brain Research* **40,** 187–192.

Vieira TM, Merletti R & Mesin L (2010). Automatic segmentation of surface EMG images: Improving the estimation of neuromuscular activity. *J Biomech* **43,** 2149–2158.

Westgaard RH & De Luca CJ (2001). Motor control of low-threshold motor units in the human trapezius muscle. *J Neuropathol* **85,** 1777–1781.

Wickham JB & Brown JMM (1998). Muscles within muscles: the neuromotor control of intra-muscular segments. *Eur J Appl Physiol* **78,** 219–225.

Wickham JB & Brown JMM (2012). The function of neuromuscular compartments in human shoulder muscles. *J Neurophysiol* **107,** 336–345.

Woods JJ & Bigland-Ritchie B (1983). Linear and non-linear surface EMG/force relationships in human muscles. An anatomical/functional argument for the existence of both. *Am J Phys Med* **62,** 287–299.

Yao W, Fuglevand RJ & Enoka RM (2000). Motor-Unit Synchronization Increases EMG Amplitude and Decreases Force Steadiness of Simulated Contractions. *Journal of Neurophysiology* **83,** 441–452.

AUTHOR CONTRIBUTIONS

- Conceptualization: JGI, SR, HVC, CRD, FN
- Data curation: JGI, SR, HVC
- Formal analysis: JGI, SR, HVC
- Funding acquisition: JGI, FN
- Investigation: JGI, SR, CC
- Methodology: JGI, SR, HVC, RP, CRD, FN
- Project administration: FN
- Writing – original draft: JGI, SR, HVC, FN
- Writing – review and editing: JGI, SR, HVC, CC, RP, CRD, FN